Nuclear Inst. and Methods in Physics Research, A 1002 (2021) 165262

Contents lists available at ScienceDirect

Nuclear Inst. and Methods in Physics Research, A

journal homepage: www.elsevier.com/locate/nima

Peak-searching method for low count rate γ spectrum under short-time measurement based on a generative adversarial network

Sunci Wu [a], Xiaobin Tang [a,b], Pin Gong [a,b,*], Peng Wang [c], Dajian Liang [a], Yong Li [a], Cheng Zhou [d], Xiaoxiang Zhu [d]

[a] Department of Nuclear Science and Technology, Nanjing University of Aeronautics and Astronautics, Nanjing 210016, China
[b] Key Laboratory of Nuclear Technology Application and Radiation Protection in Astronautics, Ministry of Industry and Information Technology, Nanjing 210016, China
[c] School of Environmental and Biological Engineering, Nanjing University of Science and Technology, Nanjing 210094, China
[d] Jiangsu Nuclear and Radiation Safety Supervision and Management Center, Nanjing 210019, China

ARTICLE INFO

Keywords:
Gamma spectrum analysis
Peak searching
Generative adversarial network
Symmetric zero-area
Nuclide identification

ABSTRACT

In scenarios such as vehicle radioactivity monitoring and unmanned aerial vehicle radioactivity monitoring, the count rate of the γ spectrum detected by the NaI(Tl) detector is low, the characteristic peak is weak, and the statistical fluctuation is large. When such a γ spectrum is processed with the conventional peak-searching method, the characteristic peak recognition accuracy is low and the nuclide identification rate is reduced. A peak-searching method based on the generative adversarial network (GAN) is proposed in this study for low count rate and short-time measurement of a single nuclide γ spectrum. Compared with the symmetric zero-area (SZA) method, the characteristic peak recognition accuracy of the GAN method is improved, the occurrence probability of false peaks is reduced, and the number of false peaks is decreased. Furthermore, the peak position offset with different time measurement conditions of the GAN method is stable. And the performance under shielding conditions of the GAN method is also better than that of the SZA method.

1. Introduction

The NaI(Tl) detector has many advantages such as mature preparation techniques, low cost, high gamma-ray detection efficiency, and high luminous efficiency. It is widely used in γ spectrum detection [1]. However, the energy resolution of the detected γ spectrum is low [2,3]. The key in the analysis of the γ spectrum is to calculate and determine the position of each characteristic peak accurately. In scenarios such as vehicle radioactivity monitoring and unmanned aerial vehicle radioactivity monitoring, the radioactive activity may be small or the detection distance is generally large. Thus, the count rate of the γ spectrum detected by the NaI(Tl) detector is low and the characteristic peak is weak. In addition, in these scenarios, the measurement time is usually short to improve the detection range and efficiency, the statistical fluctuation of the measured energy spectrum is large [4–6].

The symmetric zero-area (SZA) method is a fast, sensitive and straightforward method for peak searching. It has good recognition capability for weak and overlapping peaks and has been widely used in peak searching program or other applications [7–11]. The basic idea is to perform convolution transformation between the zero-area 'window' function and the measured spectrum data. The convolutional transformation of a linear substrate is zero, the convolutional transformation of the characteristic peak is not zero [12,13]. However, the SZA method is also affected by smoothing processing to a certain extent. Given the increasing demand for rapid nuclide recognition, a peak-searching method with improved performance needs to be developed.

The artificial neural network has been the most widely used technology in artificial intelligence in the past 10 years. The generative adversarial network (GAN) is a new type of artificial neural network. It produces good results in image synthesis, speech synthesis, and text synthesis [14,15]. In this study, we propose the use of GAN to process the low count rate γ spectrum detected with a short time.

2. Methods and experiments

2.1. Overview

The proposed peak-searching algorithm based on GAN has two parts (Fig. 1), (a) GAN training and (b) peak searching test using the trained network.

A schematic of GAN training is shown in Fig. 1(a). The training process includes two parts. (1) Obtaining the sample sets. The sets

* Corresponding author at: Department of Nuclear Science and Technology, Nanjing University of Aeronautics and Astronautics, Nanjing 210016, China.
E-mail address: gongpin@nuaa.edu.cn (P. Gong).

https://doi.org/10.1016/j.nima.2021.165262
Received 29 December 2020; Received in revised form 16 March 2021; Accepted 18 March 2021
Available online 27 March 2021
0168-9002/

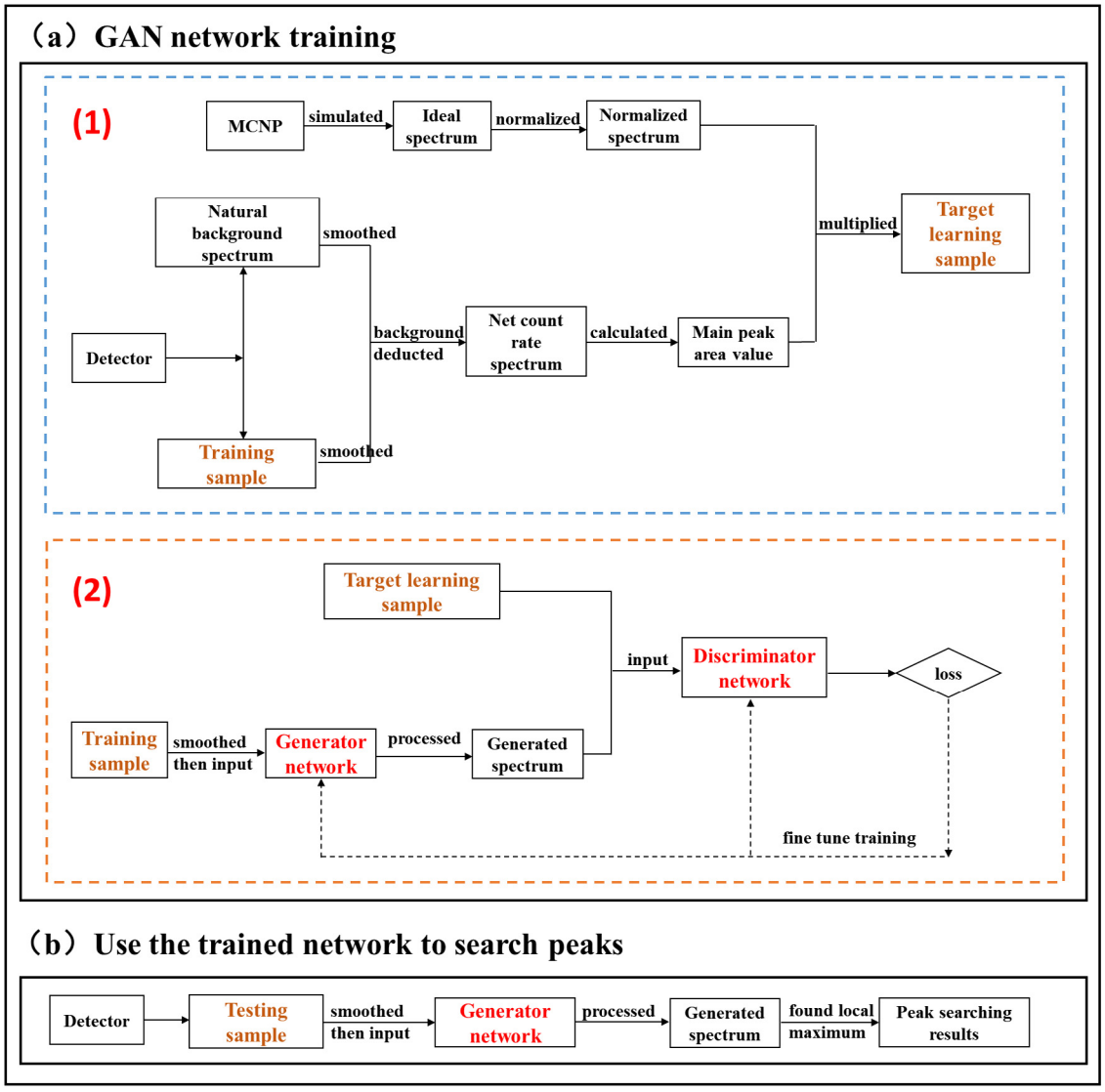

Fig. 1. Schematic of the proposed algorithm. (a) GAN training and (b) use of the trained network to search peaks.

of training sample and target learning sample are required for network training. The training sample can be obtained through direct measurement with the detector. The target learning sample is mainly obtained through the following steps. First, the ideal spectrum is obtained through MCNP simulation. And the ideal spectrum is normalized setting the highest peak to 1. Second, wavelet transform is used to smooth the natural background spectrum and the training sample [16], then background subtraction is performed and then the highest characteristic peak area is calculated. Third, the peak area value is multiplied by the normalized spectrum to get the target learning sample. (2) Training the network. The training sample sets are smoothed by wavelet transform and then inputted into the generator network, which outputs the generated spectra. Next, the generated spectra and the target sample sets are inputted into the discriminator network, which calculates the difference between the generated spectrum and the target learning sample. The error is fed back, and fine tune training is performed.

A schematic of the peak-searching test of the trained network is shown in Fig. 1(b). First, the γ spectra different from the training sample sets are measured as testing samples. After wavelet transform smoothing, the testing sample sets are inputted into the trained generator network, which outputs the generated spectra. Then, the peak position is determined by finding the local maximum value in the generated spectra.

2.2. GAN model

GAN is mainly composed of two parts: generator and discriminator networks. The generator network is to generate new data based on the characteristics of the input data. In this study, U-Net model was used as the basic framework of the generator network. U-Net has strong feature extraction capability, which can extract features from shallow to very deep levels [17]. The network was optimized for the energy spectrum, and was finally designed with an eight-layer down-sampling and up-sampling network structure. The specific network structure, related parameters and activation functions are shown in Fig. 2(a). The discriminator network is to evaluate the effect of generated spectrum, and it was designed with four convolutional layers and a fully connected layer here. The specific network structure, related parameters and activation functions are shown in Fig. 2(b).

The program running environment was as follows: TensorFlow-CPU version was 1.31.1, Keras version was 2.1.3, Python version was 3.7, the training epoch was set to 20,000, and the batch size was set to 64.

2.3. Sample acquisition

In this study, seven types of radionuclides commonly used in the industry were studied [18]. The seven types are ^{241}Am, ^{133}Ba, ^{57}Co,

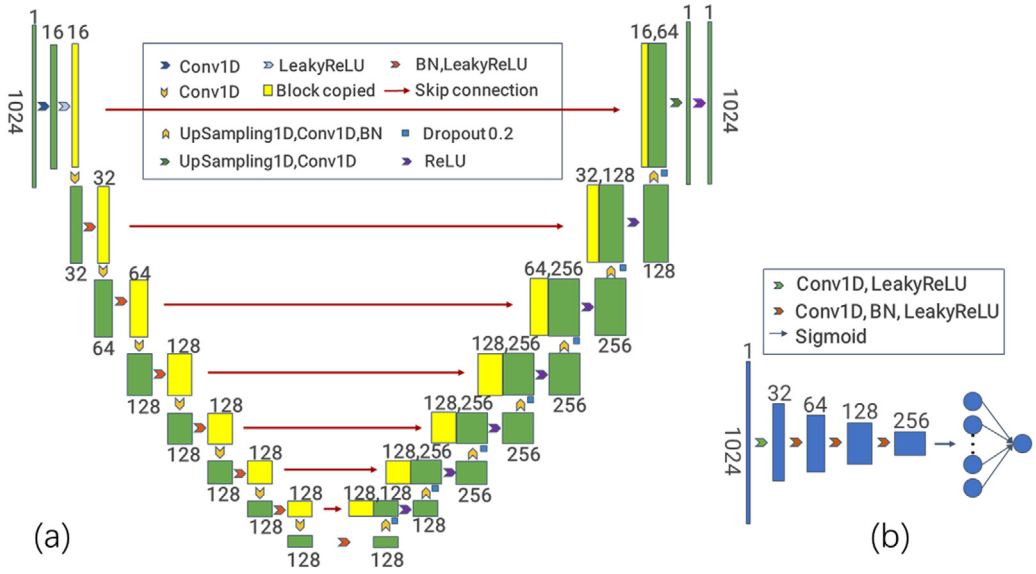

Fig. 2. (Color online) (a) Generator network structure framework and (b) discriminator network structure framework.

Table 1
Characteristic peak energy and branch ratio of seven nuclides.

Nuclides	Characteristic peak energy /KeV (Branch ratio/%)	Nuclides	Characteristic peak energy /KeV (Branch ratio/%)	Nuclides	Characteristic peak energy /KeV (Branch ratio /%)
^{241}Am	59.5(35.9)	^{60}Co	1332.5(99.986) 1173.2(99.974)		121.8(28.4) 344.3(26.6)
^{133}Ba	356(62.2) 81(34.2) 302.9(18.4)	^{137}Cs	661.7(85.2)	^{152}Eu	1408(20.8) 1112.1(13.6) 778.9(13)
^{57}Co	122.06(85.6) 136.47(10.68)	^{238}Pu	43.5(0.0395)		1085.9(9.9) 244.7(7.5)

Table 2
Activity table of seven radioactive sources.

Nuclides	^{241}Am	^{133}Ba	^{57}Co	^{60}Co	^{137}Cs	^{152}Eu	^{238}Pu
Numbering	AM-001	BA-001	C7–002	CO-008	CS-008	EU-001	P8-002
Activity/Ci	2.54E−7	9.68E−6	4.16E−6	1.89E−7	1.17E−6	1.15E−5	8.78E−3

^{60}Co, ^{137}Cs, ^{152}Eu, and ^{238}Pu. The characteristic peak energy and branch ratio are shown in Table 1. The activity of the radioactive sources used in the experiment is shown in Table 2.

2.3.1. Obtaining the training and testing samples

The radioactive source was measured with different distances and times. The background spectrum was first detected for 5 min. The net count rate of the highest characteristic peak was made equivalent to replace the detection distance because the activity of each radioactive source was different. The schematic of the experimental detection is shown in Fig. 3. The detecting distances for each radioactive source are shown in Table 3.

Two locations with a net count rate of 5 and 15 cps were recorded for each radioactive source. Five positions were randomly selected between the two locations. In each position, the detector measured 5, 10, 15, 20, and 25 s, and the measurement was repeated twice. A total of 350 sets of γ spectra were formed as the training samples. In addition, the background spectra of 5, 10, 15, 20, and 25 s were measured respectively, and each time period was measured 3 times. They were used later to generate the target learning samples.

The testing samples were different from the training samples. Three locations with a net count rate of 5, 10 and 15 cps were recorded for each radioactive source. In each location, the detector measured 2, 3, 5, 10, 15, and 20 s. A total of 126 sets of γ spectra were formed as the testing samples.

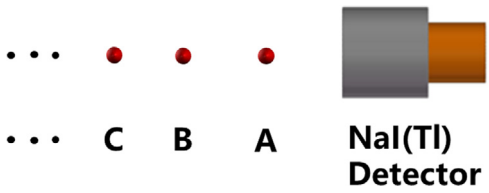

Fig. 3. Schematic of the experimental detection of radioactive sources, A, B, and C represent different detection positions.

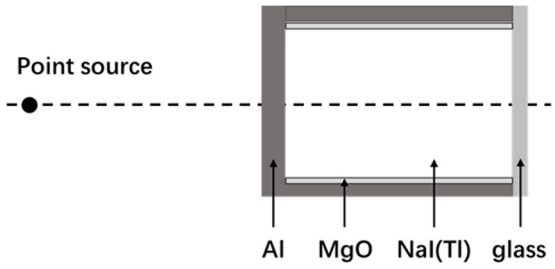

Fig. 4. Simplified NaI(Tl) detector model.

2.3.2. Obtaining the target learning samples

A simplified Monte Carlo model was established (Fig. 4) based on the NaI(Tl) detector used. The crystal size was 2×2 inches. It was wrapped with an aluminum shell. The thickness of the front was 0.25 cm, the side was 0.2 cm, the MgO reflection layer was 0.05 cm, and the glass was 0.2 cm.

Table 3
Detecting distances for each radioactive source.

Nuclides	Background count rate /cps	Net count rate /cps	Distance /cm	Nuclides	Background count rate /cps	Net count rate /cps	Distance /cm
		5.25	37.2			5.37	131.8
^{241}Am	9.31	10.3	22.8	^{152}Eu	8.55	10.33	92.3
		14.05	18.4			15.63	83.5
		4.9	53.7			5.7	133
^{137}Cs	3.19	9.4	41.6	^{57}Co	20.00	11.1	93
		14.6	33.2			14.75	87
		5.83	11.8			5.37	75.2
^{60}Co	1.00	9.1	9.0	^{238}Pu	14.98	9.93	61.2
		14.8	6.7			14.07	55.3
		6.57	147.0				
^{133}Ba	7.08	9.1	126.1				
		14.27	107.6				

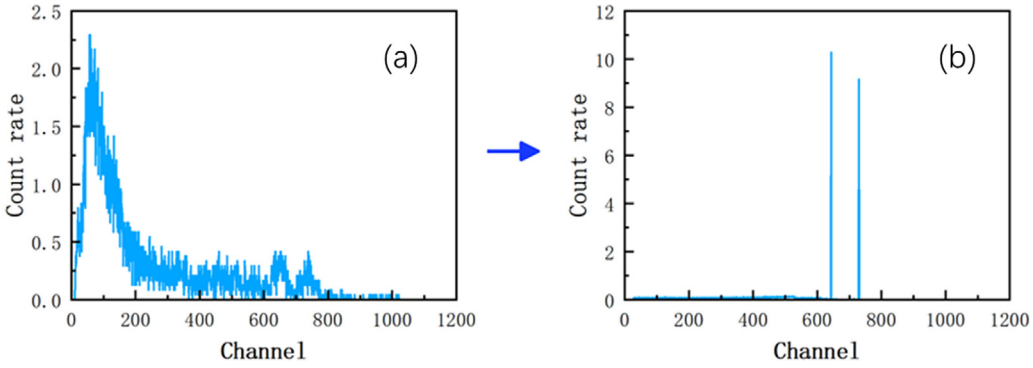

Fig. 5. (a) Measured ^{60}Co γ spectrum and (b) the corresponding target learning γ spectrum.

MCNP5 was used to perform a simulation and the ideal γ spectra of seven nuclides were obtained [19]. Then, the method mentioned in Section 2.1 was used to generate the target learning γ spectra. A total of 350 sets of target learning samples were formed. An example of the training sample and its target learning sample of ^{60}Co is shown in Fig. 5.

2.3.3. Obtain the testing samples under shielding conditions

As shown in Fig. 6, for each nuclide, the radioactive source was placed at the location with the net count rate of 15cps recorded in Section 2.3.1. Next, the shielding material (5 mm steel, 10 mm steel, 5 mm lead, and 10 mm lead) was placed 2 cm away from the radioactive source. The detector measured for different times (3, 5, 10, 15, 20, and 30 s for the steel condition; 3, 5, 10, 30, 60, and 120 s for the lead condition). A total of 168 sets of γ spectra were formed.

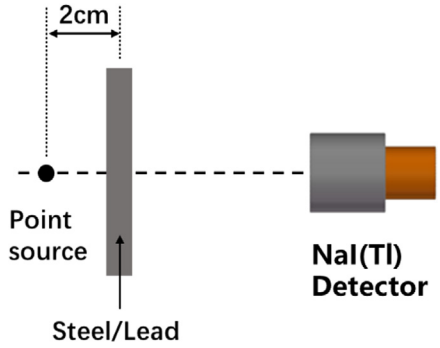

Fig. 6. Schematic of detection with a shielding material.

2.4. Data processing and analysis

The process of the SZA method is shown in Fig. 7. First, the background subtraction of the testing samples is performed. Second, the testing samples are processed using the SZA algorithm. Lastly, the peak position is determined by finding the local maximum value in the processed spectra.

The parameters of the optimal local maximum algorithm with the two methods were determined. The possible characteristic peaks were searched by the algorithm. When the ratio of the difference between the recorded peak energy and the searched peak energy to the recorded peak energy was less than the energy window, the peak was considered to belong to a certain nuclide, and the rest were considered false peaks [20,21]. Through the pre-experiment, the energy window size was set to 2%.

3. Results and discussion

The training samples in Section 2.3.1 and the target learning samples in Section 2.3.2 were used as training datasets for GAN training. After the training was completed, the testing samples in Section 2.3.1 were processed by the trained GAN and the SZA method. The peak recognition results are shown in Section 3.1, and the peak position offset results are shown in Section 3.2. The testing samples measured under the shielding conditions in Section 2.3.3 were processed by the two methods. The results are shown in Section 3.3.

3.1. Characteristic peak recognition results

Determining the peak position of each peak is crucial in the analysis of the γ spectrum. The more searched characteristic peaks belong to the nuclide, the more likely the nuclide exists. The results are shown below.

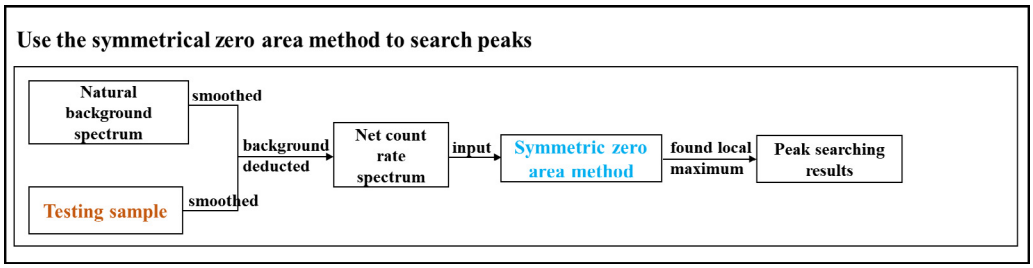

Fig. 7. Schematic of the SZA method for peak searching.

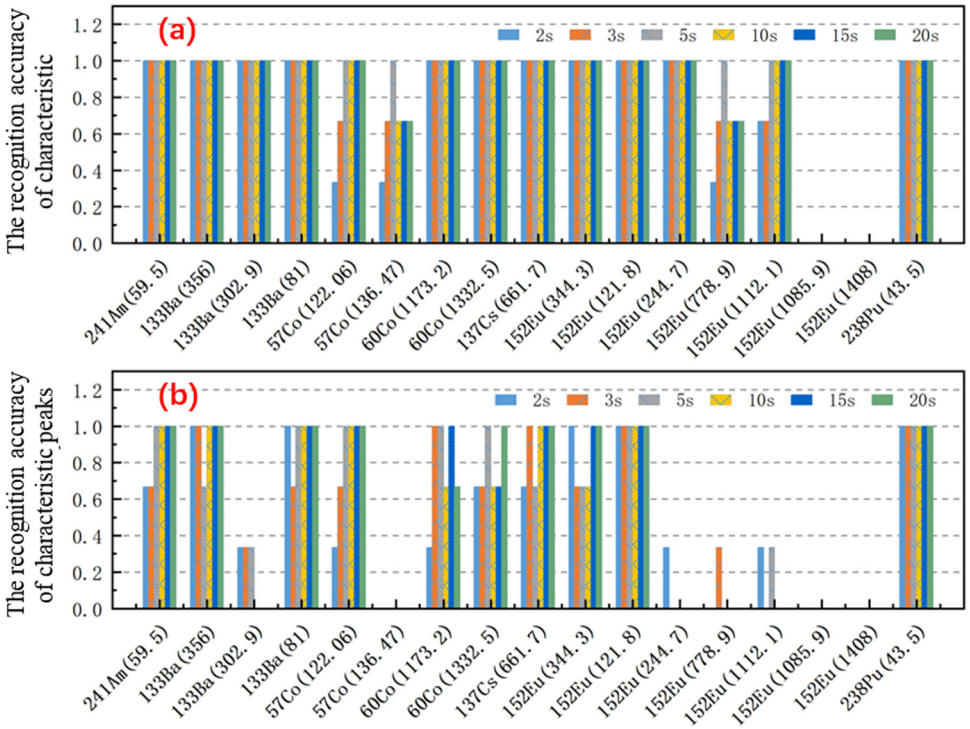

Fig. 8. (Color online) Recognition accuracy of characteristic peaks after peak-searching for the γ spectrum under each time measurement condition of each nuclide. (a) GAN method results and (b) SZA method results.

Fig. 8 indicates that the characteristic peak recognition accuracy of the GAN method (an average of 82.68%) was generally higher than that of the SZA method (an average of 54.58%). The GAN method could accurately search for the characteristic peaks of ^{241}Am, ^{133}Ba, ^{60}Co, ^{137}Cs, and ^{238}Pu in all the measured γ spectra. However, the SZA method could only accurately search for the characteristic peaks of ^{238}Pu in the measured γ spectra.

Several failure cases were encountered when the GAN method was used to search for the characteristic peaks of ^{57}Co. A possible reason is that the two characteristic peaks (energies of 122.06 and 136.74 KeV) are close, as shown in Fig. 9(a). Overlapping peaks affect the judgment of peak positions. Correspondingly, when the measured γ spectrum of this nuclide was processed by the SZA method, the characteristic peak with the energy of 136.74 KeV could not be found. The GAN method is better than the SZA method in dealing with overlapping peaks.

For ^{152}Eu, peak searching of the GAN method failed in some cases with the characteristic peaks (energies of 778.9 and 1112.1 KeV) and failed in all cases with the characteristic peaks (energies of 1085.9 and 1408 KeV). A possible reason is that the four characteristic peaks are weak and have large statistical fluctuations under a short time measurement, as shown in Fig. 9(b). Thus, the peak searching algorithm cannot judge the peak position well. Besides, there is a partial overlap between the two characteristic peaks with energies of 1085.9 and 1112.1 KeV. Correspondingly, when the measured γ spectrum of this nuclide was processed by the SZA method, the characteristic peaks with energies of 1085.9 and 1408 KeV could not be found, and only with a few cases the characteristic peaks with energies of 778.9 and 1112.1 KeV could be found. The GAN method is slightly better than the SZA method in dealing with weak peaks.

Fig. 10 shows that the overall occurrence probability of false peaks was low (only 16.67% on the average) with the GAN method. Meanwhile, the occurrence probability of false peaks was as high as 86.51% with the SZA method. For each nuclide, the occurrence probability of false peaks of the GAN method was lower than that of the SZA method.

Fig. 11 indicates that the number of false peaks of the GAN method (approximately 0.17 on the average) was much smaller than that of the SZA method (approximately 2.06 on the average). For every single nuclide and each time measurement condition, the average number of false peaks of the GAN method was much smaller than that of the SZA method. The GAN method could easily identify the characteristic peaks after processing, and the interference of false peaks was minimal. The interference of false peaks in the SZA method was high, which would affect the determination of the characteristic peaks of the nuclides. When the measurement time increased, the number of false peaks decreased.

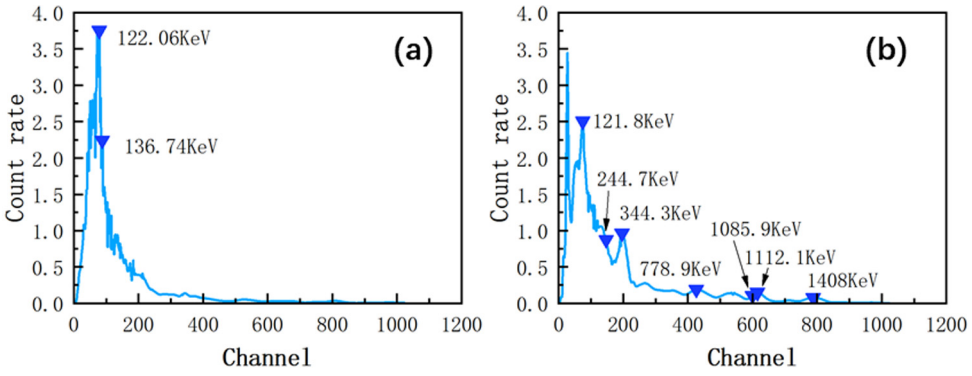

Fig. 9. (a) Measured peak position of the γ spectrum under the measurement condition of 15 cps+20 s for ^{57}Co. (b) Measured peak position of the γ spectrum under the measurement condition of 15 cps+20 s for ^{152}Eu.

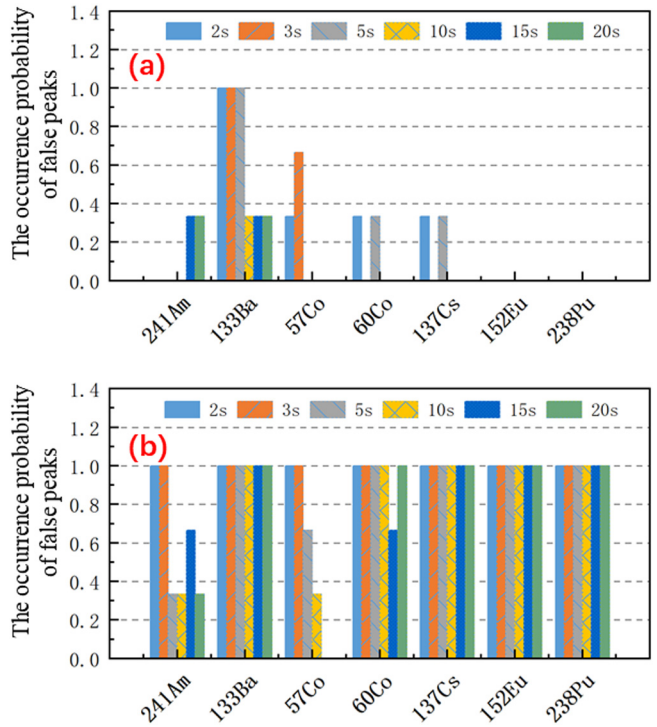

Fig. 10. (Color online) Occurrence probability of false peaks after peak-searching of the γ spectrum under each time measurement condition of each nuclide. (a) GAN method results and (b) SZA method results.

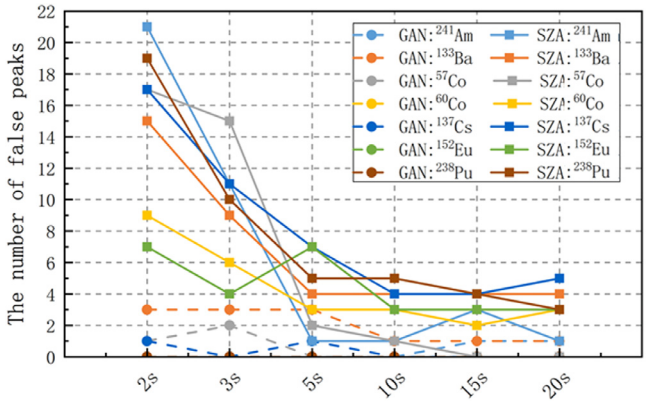

Fig. 11. (Color online) Number of false peaks after peak-searching of the γ spectrum of each nuclide at each time measurement.

3.2. Characteristic peak position offset results

The size of the energy window has a great influence on nuclide identification and an appropriate energy window size should consider the peak position offset. The results are shown below.

As shown in Fig. 12, excluding the characteristic peaks that could not be found, the peak position offset of the GAN method was about 0.4% on the average. In consideration of the maximum offset, the energy window should be set to 1.2%. The average peak position offset of the SZA method was small at about 0.2%. However, the peak position changed under different time measurement conditions. In consideration of the fluctuations, the energy window should be set to 1%.

For the GAN method, the peak position did not fluctuate under different time measurement conditions except for ^{241}Am and ^{60}Co. The small cases of the peak position fluctuations of the two nuclides may be due to the uncertainty of the γ spectrum statistics.

In general, the energy window size for the GAN method is close to the SZA method. And we find that the peak position under different time measurement conditions of the GAN method is more stable than that of the SZA method. With this feature, we can correct the peak searching results to improve the accuracy of characteristic peak recognition.

3.3. Processing results of testing samples under shielding conditions

The testing samples measured under the shielding condition were processed by the two methods, and the results are shown below.

Fig. 13 (a) indicates that with the same shielding material, the characteristic peak recognition accuracy of the GAN method was higher than that of the SZA method. The average recognition accuracy of characteristic peaks for the different shielding materials was 5 mm steel > 10 mm steel, 5 mm lead > 10 mm lead. Fig. 13(b) indicates that the average occurrence probability of false peaks of the GAN method was much lower than that of the SZA method. For the GAN method, the average false peak occurrence probability of the four shielding materials remained low. Fig. 13(c) shows that the total number of false peaks of the GAN method was smaller than that of the SZA method, which had little impact on the judgment of characteristic peaks. For the GAN method, the average number of false peaks of the four shielding materials remained small.

The number of searched characteristic peaks of 7 nuclides under different time measurement conditions was counted. The total number of characteristic peaks of 7 nuclides should be 17, as shown in Table 1. The results are shown in Fig. 14.

As shown in Fig. 14, given the same shielding material, the number of characteristic peaks identified by the GAN method was bigger than

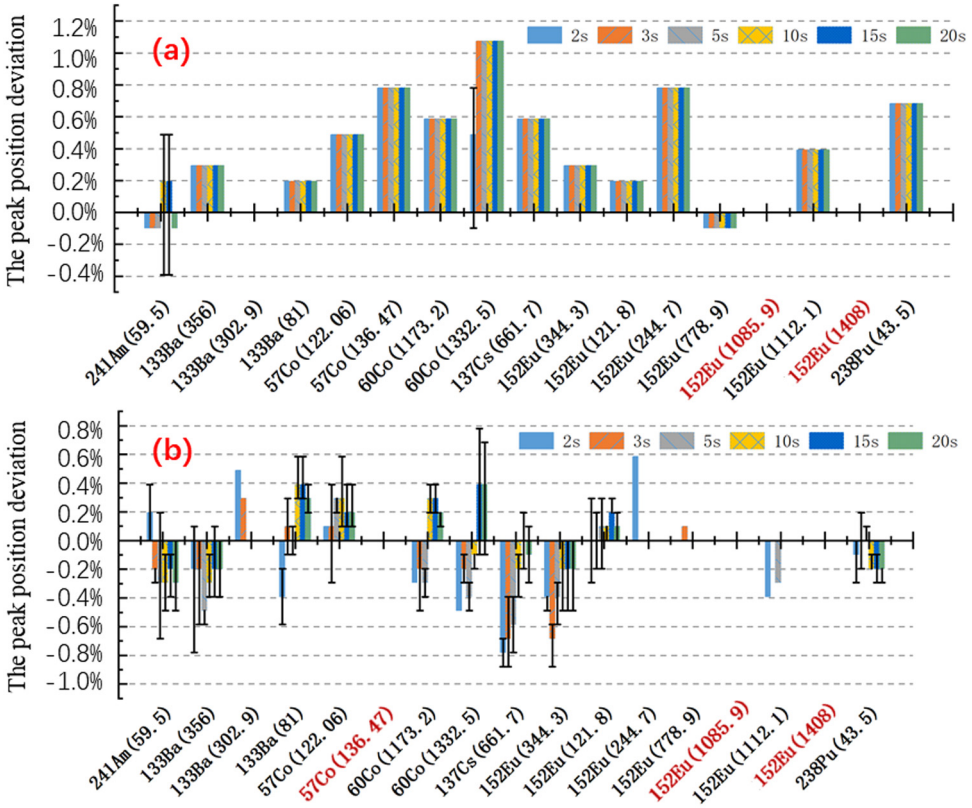

Fig. 12. (Color online) Peak position deviation of each nuclide. The height of the column represents the average offset of all the determined characteristic peaks of the nuclide. A positive value represents the left offset, and a negative value represents the right offset; the two ends of the vertical line represent the maximum and minimum offsets. For the characteristic peaks, shown in red on the horizontal axis, cannot be found and therefore no peak position deviation is observed. (a) GAN method results and (b) SZA method results.

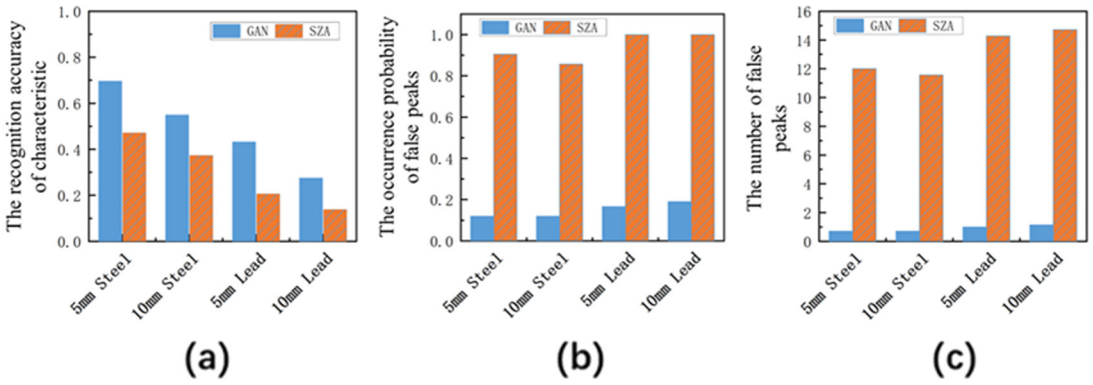

Fig. 13. (a) Average recognition accuracy of characteristic peaks, (b) average occurrence probability of false peaks, and (c) average number of false peaks.

that identified by the SZA method. With the increase in measurement time, the number of identified characteristic peaks increased slightly then flattened.

4. Conclusion

A peak-searching method of low count rate γ spectrum under short-time measurement based on GAN was proposed. The research results prove that the proposed method improves the recognition accuracy of characteristic peaks, reduces the occurrence probability of false peaks, and decreases the number of false peaks when processing low count rate γ spectrum under short-time measurement.

When dealing with low count rate γ spectrum under short-time measurement in this study, the proposed method has these advantages. (1) The peak recognition accuracy of characteristic peaks is higher compared with the SZA method and the performance of processing overlapping and weak peaks is better. (2) The occurrence probability of false peaks is lower and the number of false peaks is smaller. (3) The average offset rate of the GAN method is higher than that of the SZA method, but the offset is more stable. The SZA method has large offset fluctuations. For the GAN method, the feature of offset stability can be used to correct the peak searching results. (4) Under the shielding condition, the recognition accuracy of characteristic peaks of the GAN method is higher than that of the SZA method. For different shielding materials, the average recognition accuracy of characteristic peaks is 5 mm steel > 10 mm steel, 5 mm lead > 10 mm lead. Meanwhile, the average occurrence probability of false peaks and the average number of false peaks of the GAN method are much lower and smaller than those of the SZA method.

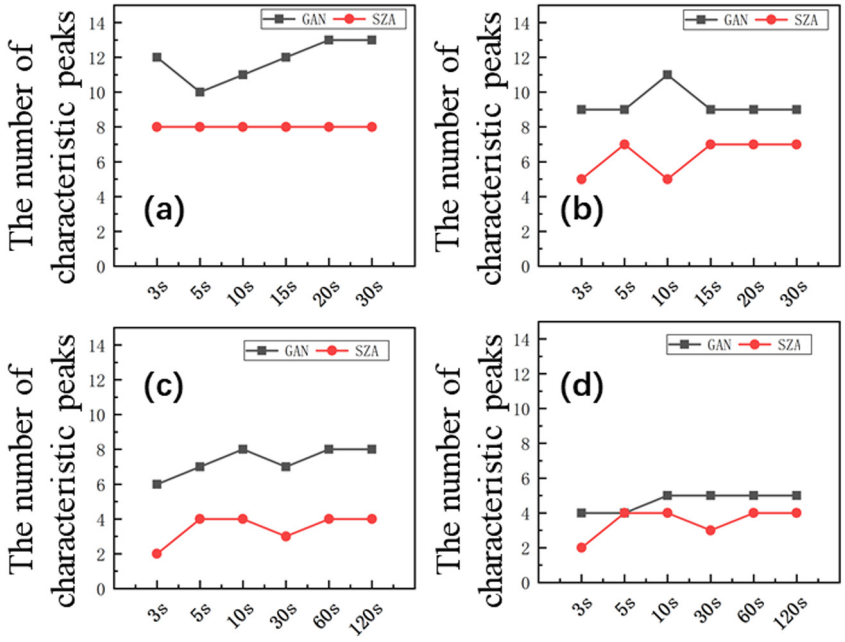

Fig. 14. (a) Accurate identification of characteristic peaks for 5 mm steel, (b) 10 mm steel, (c) 5 mm lead, and (d) 10 mm lead.

The proposed method has limitations. The trained network in this study cannot accurately search for other untrained peaks. Future work will study more nuclides and quantitative calculation of nuclide activity.

CRediT authorship contribution statement

Sunci Wu: Software, Validation, Writing - original draft. **Xiaobin Tang:** Methodology, Validation. **Pin Gong:** Conceptualization, Writing - review & editing. **Peng Wang:** Data curation, Investigation. **Dajian Liang:** Methodology, Software. **Yong Li:** Visualization, Investigation. **Cheng Zhou:** Visualization, Software. **Xiaoxiang Zhu:** Investigation, Validation.

Declaration of competing interest

The authors declare that they have no known competing financial interests or personal relationships that could have appeared to influence the work reported in this paper.

Acknowledgments

This work was supported by the Primary Research and Development Plan of Jiangsu Province, China (Grant No. BE2019727), the Fundamental Research Funds for the Central Universities, China (Grant No. NT2020017), the Foundation of Graduate Innovation Center in NUAA, China (Grant No. kfjj20200611).

References

[1] B.D. Milbrath, A.J. Peurrung, M. Bliss, W.J. Weber, Radiation detector materials: An overview, J. Mater. Res. 23 (2008) 2561–2581.
[2] J. Wang, Y. Zhang, D. Liu, B. Wu, Y. Zhang, H. Jiang, Automated spectra analysis of in situ radioactivity measurements in the marine environment using NaI(Tl) detector, Appl. Radiat. Isot. 141 (2018) 88–94.
[3] E.R. Siciliano, J.H. Ely, R.T. Kouzes, B.D. Milbrath, J.E. Schweppe, D.C. Stromswold, Comparison of PVT and NaI(Tl) scintillators for vehicle portal monitor applications, Nucl. Instrum. Methods Phys. Res. A 550 (2005) 647–674.
[4] J.I. Young-Yong, K. Ho Chung, M. Ja Kang, Assessment of dose rate of detected gamma emitting nuclides using a carborne survey with a large volume NaI(Tl) detector, Prog. Nucl. Energy 123 (2020) 103272.
[5] S. Guguła, K. Kozak, J. Mazur, D. Grządziel, M. Mroczek, Fast in situ gamma spectroscopy using hand-held spectrometer with NaI probe, J. Environ. Radioact. 188 (2018) 87–94.
[6] X. Bin Tang, J. Meng, P. Wang, Y. Cao, X. Huang, L.S. Wen, D. Chen, Efficiency calibration and minimum detectable activity concentration of a real-time UAV airborne sensor system with two gamma spectrometers, Appl. Radiat. Isot. 110 (2016) 100–108.
[7] J. Uher, G. Roach, J. Tickner, Peak fitting and identification software library for high resolution gamma-ray spectra, Nucl. Instrum. Methods Phys. Res. 619 (2010) 457–459.
[8] R. Luo, Y. Huang, X. Liu, Comparative study on peak-seeking methods of the mixed radioactive energy spectrum, OALib. 07 (2020) 1–10.
[9] Y.Z. Yang, F. Fang, J.F. He, J.J. Ran, A study of the peak boundary method and effect evaluation based on NaI(TI) detector for γ-spectrum analysis, Appl. Mech. Mater. 347–350 (2013) 1006–1011.
[10] F. Li, Z. Gu, L. Ge, H. Li, X. Tang, X. Lang, B. Hu, Review of recent gamma spectrum unfolding algorithms and their application, Results Phys. 13 (2019).
[11] M. Morháč, An algorithm for determination of peak regions and baseline elimination in spectroscopic data, Nucl. Instrum. Methods Phys. Res. 600 (2009) 478–487.
[12] G.W. Phillips, K.W. Marlow, Automatic analysis of gamma-ray spectra from germanium detectors, Nucl. Instrum. Methods 137 (1976) 525–536.
[13] J. He, S. Huang, Z. Ye, X. Wang, X. Li, S. Zhou, A Study of Combined Peak-Searching Method for Symmetric Zero Area and Gaussian Product Function Based on G-Ray Spectrum, Vol. 173, 2018, pp. 131–137.
[14] I.J. Goodfellow, J. Pouget-Abadie, M. Mirza, B. Xu, D. Warde-Farley, S. Ozair, A. Courville, Y. Bengio, Generative adversarial networks, 2014, ArXiv.
[15] A. Radford, L. Metz, S. Chintala, Unsupervised representation learning with deep convolutional generative adversarial networks, 2016, ArXiv.
[16] J. He, X. Tang, P. Gong, P. Wang, L. Wen, X. Huang, Z. Han, W. Yan, L. Gao, Rapid radionuclide identification algorithm based on the discrete cosine transform and BP neural network, Ann. Nucl. Energy 112 (2018) 1–8.
[17] O. Ronneberger, P. Fischer, T. Brox, U-net: Convolutional networks for biomedical image segmentation, 2015, ArXiv.
[18] International Atomic Energy Agency, Technical and functional specifications for border monitoring equipment, 2006.
[19] T. Sharshar, M.L. Hussein, An optimization of energy window settings for positron annihilation lifetime spectrometers, Nucl. Instrum. Methods Phys. Res. 546 (2005) 584–590.
[20] S.Z. Islami rad, Optimization of energy window for gamma densitometer based backscatter method in oil industry, Russ. J. Nondestruct. Test. 52 (2016) 245–249.
[21] X-5 Monte Carlo Team, MCNP - A general Monte Carlo n-particle transport code, version 5, 2003.